PERGAMON

International Journal of Impact Engineering 28 (2003) 137–160

INTERNATIONAL JOURNAL OF IMPACT ENGINEERING

www.elsevier.com/locate/ijimpeng

Response of hot isostatically pressed Ti–6Al–4V targets to normal impact by conical and blunt projectiles

V.F. Nesterenko[a,*], W. Goldsmith[b], S.S. Indrakanti[a], YaBei Gu[a]

[a] *University of California, San Diego, USA*
[b] *University of California, Berkeley, USA*

Received 12 November 2001; received in revised form 7 June 2002

Abstract

First experimental results are reported on ballistic performance of hot isostatically pressed (HIPed) texture-free targets using rapidly solidified powders of Ti–6Al–4V alloy (PREP and ELI-PREP). Plastic deformation by ball milling of these powders was performed to modify the microstructure of the materials. HIPed samples of 40 mm diameter and a thickness of 10–30 mm were shrinkfit into holes in larger diameter steel plates and struck by 50 caliber 60° cylindro-conical projectiles of hardness R_c 60 with contact produced either by the conical or blunt surface. The mass of the projectile was about 31 g and the initial velocities ranged from 300 to 450 m/s for flat-ended and from 900 to 950 m/s for the conical impacts. Comparative behavior of HIPed samples and standard samples made from commercially available Ti–6Al–4V alloy MIL-T-9047G (bar, forged, annealed)—baseline material after impact with the same geometry was investigated. As a rule the final velocity of the plug for HIPed alloy was smaller (or no penetration was observed) than that of the baseline material for impact with the conical projectile. Slightly sloped cylindrical shear plugs were characteristic for both materials upon impact by flat projectiles and their velocities were used to evaluate the shear resistance of HIPed material to plugging. Comparative features of fracture in both cases are presented. The texture-free HIPed materials from powders demonstrated better ballistic performance than the baseline material and could be successfully used for ballistic applications. This is the first step in the development of high-gradient composite materials using a Ti–6Al–4V matrix from powder.

Keywords: Hot isostatically pressed titanium alloys; Ballistic performance; Plugging; Shear localization

*Corresponding author. Fax: +1-858-534-5698.
E-mail address: vnesterenko@ucsd.edu (V.F. Nesterenko).

0734-743X/02/$ - see front matter
PII: S0734-743X(02)00052-0

1. Introduction

Ballistic penetration has been a subject of concern in the military and technological communities for over 250 years and was pursued by many of the greats of mechanics and physics including Newton, Hooke, Euler, Cauchy and others (see historical review in [1–5]). The objective of these investigations has been the assessment of materials to provide maximum protection under attack by projectiles. This was accomplished by the firing of strikers of certain geometry and material against targets; when the targets were thick, the ballistic performance of these objects was measured by the depth of penetration of the projectile. For thin targets, the performance measure was the ballistic limit, i.e. the velocity at which 50% of the strikers would just barely penetrate the target. The first mechanical model of perforation, in the case relative to the present research (plugging) was advanced by Martel [6]. More sophisticated representations of penetration phenomena taking into account material strength were proposed by Alekseevski [7].

Recently, advances in metallurgy and microscopic analysis have permitted association of material properties with penetration resistance. However, dramatic improvements in ballistic performance of shielding materials, exhibiting different microstructure, are not reflected in corresponding enhancement in properties determined from standard mechanical tests of the solid samples [8]. In recent years, Ti-alloys were studied extensively as armor materials because they provide better ballistic resistance than steel or aluminum. Ti–6Al–4V alloy with extra low interstitial (ELI) content had become the material of choice for armor applications due to its increased ductility because of the reduction of interstitial elements (C, O, N and H) [9–11].

A correlation between the ballistic behavior and dynamic properties of targets was investigated by Rupert and Grace [12], Huang et al. [13], Burkins and Love [10], Gooch and Burkins [11], Me-Bar and Rosenberg, [8], and Bless et al. [14]. Different heat treatments of Ti–6Al–4V were examined to replace shear localization and plugging by bulk deformation and bulging [15,16].

Complete and incomplete perforation processes obtained experimentally in reverse ballistic tests using rods of hard steel were analyzed to relate the observed phenomena to the measured average plugging shear resistance in Ti–6Al–4V specimens [17]. Shear localization is an important failure mechanism in high-strength metallic substances, but this is particularly so in this titanium alloy. The influence of material properties on adiabatic shear localization was investigated by Me-Bar and Shechtman [18] and Mazeau et al. [19].

No previous comparison of ballistic performance of any parent material of Ti–6Al–4V alloy and its consolidated from powder counterpart has been presented prior to the present investigation, except as reported by Nesterenko et al. [20–22]. At the same time, a powder-based technique provides a texture-free substance and constitutes a unique way to synthesize a composite material with complex internal structure including components with essentially different properties. This paper is intended to examine the ballistic resistance properties in a thermomechnically treated homogeneous plate made from a 2 in bar of Ti–6Al–4V alloy (MIL-T-9047G, forged, annealed) with clearly identified texture [24], here called the baseline material, and texture-free targets processed from compacted Ti–6Al–4V powder (PREP). Forged material was selected to provide repeatable properties of the baseline material in small-scale laboratory ballistic tests. The properties of this material provided by the manufacturers ($\sigma_{0.2} = 913$ MPa, tensile

strength 990 MPa, reduction of area 43.6% and elongation 17.5% at failure) represent probably the best combination of high strength and high ductility among Ti–6Al–4V alloys. These properties are commonly accepted as being beneficial for the ballistic performance and are significantly better than the properties of rolled plates of Ti–6Al–4V alloy manufactured to armor specification MIL-A-46077D ($\sigma_{0.2} = 793$ MPa, tensile strength 862 MPa, reduction of area 25% and elongation 12% [10]) or properties of Ti–6Al–4V armor reported in [16] (Ti–6Al–4V alloy A: $\sigma_{0.2} = 869$ MPa, UTS = 979 MPa, elongation 11%; Ti–6Al–4V alloy B: $\sigma_{0.2} = 882$ MPa, UTS = 972 MPa, elongation 16%). From this point of view the comparison with the selected baseline material will provide a reasonable estimate of the ballistic performance of corresponding material made from powder. At the same time it is probably true that the selection of baseline material based only on quasistatic (or even dynamic) properties is somewhat arbitrary because ballistic performance to a large extent is determined by dynamic postcritical behavior of the material which is not represented by quasistatic or dynamic tests.

The main purpose of this comparison of ballistic behavior is to investigate the feasibility of using powder for processing of armor-related materials. This type of processing naturally involves diffusion bonding over an initially large surface area of particle interfaces. This feature may result in large local concentration of interstitial elements (nitrogen, oxygen and others) in the vicinity of these interfaces. As a result properties of compacts may not be suitable for ballistic applications due to the strong influence of these elements on the mechanical properties [25]. No results have been reported in the literature clarifying this important subject.

In the present experiments, the projectiles (with flat and 60° cylindro-conical front surfaces) are accelerated using a powder gun at velocities in the range of 300–900 m/s. The microstructural features of baseline and powder-based materials under identical conditions of plugging were examined. Ballistic experiments, particularly with plug formation, are very desirable for the study of HIPed materials because smaller critical strains for shear localization are produced in Hopkinson bar experiments in comparison with the baseline material; critical compressive strains for localization are 0.15 and 0.3, respectively [23,24]. The results demonstrated that powder-based materials have better shear resistance than the conventional Ti–6Al–4V plate. This is the first step in the development of high-gradient composite materials [20,21] using a Ti–6Al–4V matrix derived from powder.

2. Experimental work

2.1. Processing and properties of target materials

The targets were prepared using two different approaches starting from rapidly solidified plasma rotating electrode process (PREP) and PREP ELI grade powders with low content of interstitial elements obtained from Starmet Inc., Concord, MA, USA. The powders were consolidated using hot isostatic press (QIH-3miniHIPer) of Flow Autoclave Systems, Inc., Columbus, OH, USA. The chemical composition of the initial powders is presented in Table 1. Both sets of powders were also plastically deformed in a SPEX 8000 mill for 10 min each using tungsten carbide balls in a tungsten carbide vial as described previously [26]. For the sake of convenience, the powders are designated based on the preparation conditions as

Table 1
Chemical composition (weight %) of starting powders and HIPed samples

Material	O	N	H	C
Baseline	0.16	0.021	0.0015	0.03
PNM	0.20	0.008	0.002	0.01
ENM	0.11	0.01	0.002	0.01
PNM HIPed	0.18	0.01	0.0017	0.01
PML HIPed	0.28	0.01	0.0024	0.02
EML HIPed	0.18	0.02	0.007	0.04

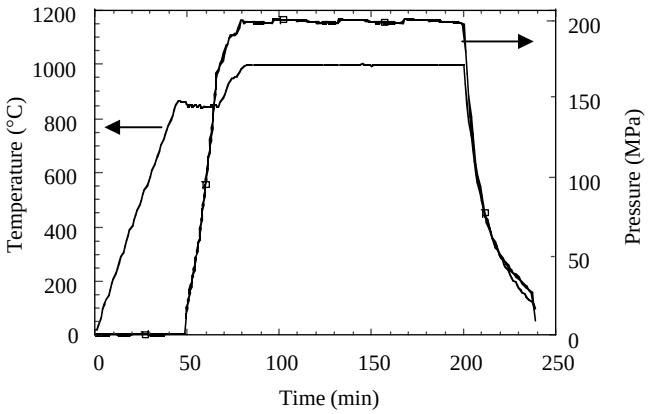

Fig. 1. Time–temperature–pressure schedule during HIPing of materials for targets for ballistic tests.

follows:

PNM-NonmilledPREPpowders, PML-MilledPREPpowders,
ENM-NonmilledELIpowders, EML-MilledELIpowders.

All powders were placed in Pyrex glass capsules of 50 mm diameter with a length of 75 mm and sealed under vacuum (10^{-2} Torr) for hot isostatic pressing (HIPing). Before sealing the glass capsules, the powders were degassed at 400°C for 4 h in a vacuum of 10^{-2} Torr.

The HIPing was carried out using argon gas in the optimized conditions established from previous research [20–22, 27]. The typical schedule for consolidation is shown in Fig. 1. Initially, the capsules were heated at low pressures ($\sim$1 MPa) up to the Pyrex glass softening temperature (850°C) and held at that temperature for 5 min. Then, argon pressure was increased to 165 MPa and the capsule was further heated up to 1000°C at 200 MPa pressure. The capsule was held at these conditions for 2 h and then cooled with simultaneous release of pressure. This HIPing schedule ensured complete densification as well as generating strength and ductility of the processed material [23].

Grinding or lathe machining removed glass on the surface of HIPed samples. The samples of 40 mm diameter and 10 or 30 mm thickness were prepared by precision machining and were assembled by press or shrink fitting into AISI 4340 steel support plates for ballistic tests by flat

and conically tipped projectiles. In a similar manner, samples with the same dimensions were also prepared from a 50.8 mm diameter forged bar of MIL-T-9047G press-fitted in steel support plates. To assess the effectiveness of the press fitting, a uniform MIL-T-9047G standard sample of 140 mm diameter was also tested.

Microstructure features such as grain size, colony size, thickness of phases, size and shape of primary α grains, texture and volume fraction of α, β phases have a strong influence on quasistatic properties like strength, ductility and toughness [25]. Under high-strain-rate loading, the microstructural effects may additionally influence adiabatic shear band initiation, growth and patterning. In the case of Ti–6Al–4V, the shear bands or voids can be initiated at α/β interfaces or at the boundary of α phases for the both Widmanstatten and equiaxed microstructure. Shear instability is one of the main fracture mechanisms in titanium alloys, which determines the postcritical behavior of the material.

Microstructures of different materials after HIPing are presented in Fig. 2 as well as the microstructure of baseline material; phase content is given in Table 2, and measurements of hardness can be found in Table 3. Measurements of sound speeds and calculated elastic modulus are shown in Table 4; corresponding quasistatic and dynamic compression Hopkinson bar data are presented in Figs. 3 and 4, respectively. Coarsening of microstructure is apparent after plastic deformation of rapidly solidified materials before HIPing (compare Figs. 2(a) and (b) and Figs. 2(c) and (d), respectively). This can be explained by increased diffusion in plastically deformed materials. Different behavior of PREP and PREP-ELI powders (compare microstructure in Figs. 2(b) and (d)) can be caused by different levels of interstitial components (see Table 1).

HIPed materials have only a slightly higher content of β phase according to the measurement (Table 2). Hardness of PML material is higher than a corresponding value for baseline material, but for other HIPed samples it is slightly lower. Elastic properties of these materials are very similar with increased value of Young's and shear modulus in the perpendicular direction for anisotropic baseline material. The results of static and dynamic compressive tests show that the baseline samples made from the perpendicular direction to the axis of the bar have higher strength but lower ductility, similar to the ductility value for the HIPed PREP-nonmilled material. It is interesting to mention that the data spread in dynamic strength and ductility for HIPed material is lower than for the baseline material. Additional data on dynamic properties of HIPed materials measured by the Hopkinson bar technique and their analysis including dependence on the initial temperature and strain rates are presented in [23,24].

2.2. Ballistic testing

The impact experiments were conducted using a 12.9 mm inside diameter barrel of a powder gun capable of firing 31 g projectiles at speeds up to 950 m/s. 50-caliber flat-ended and 60° conically tipped bullets were used in the experiments. The bullets are made from oil hardened tool steel heat treated to a hardness of 60 on the Rockwell C scale. The dimensions of the projectile are 12.73 mm diameter with an overall length of 38.1 mm and a weight of $\sim$31 g. The projectiles were coated with copper to a thickness of 0.013 mm to minimize barrel wear. The copper coating with a low shear resistance also served to clarify shear resistance to plugging inside the Ti–6Al–4V alloy,

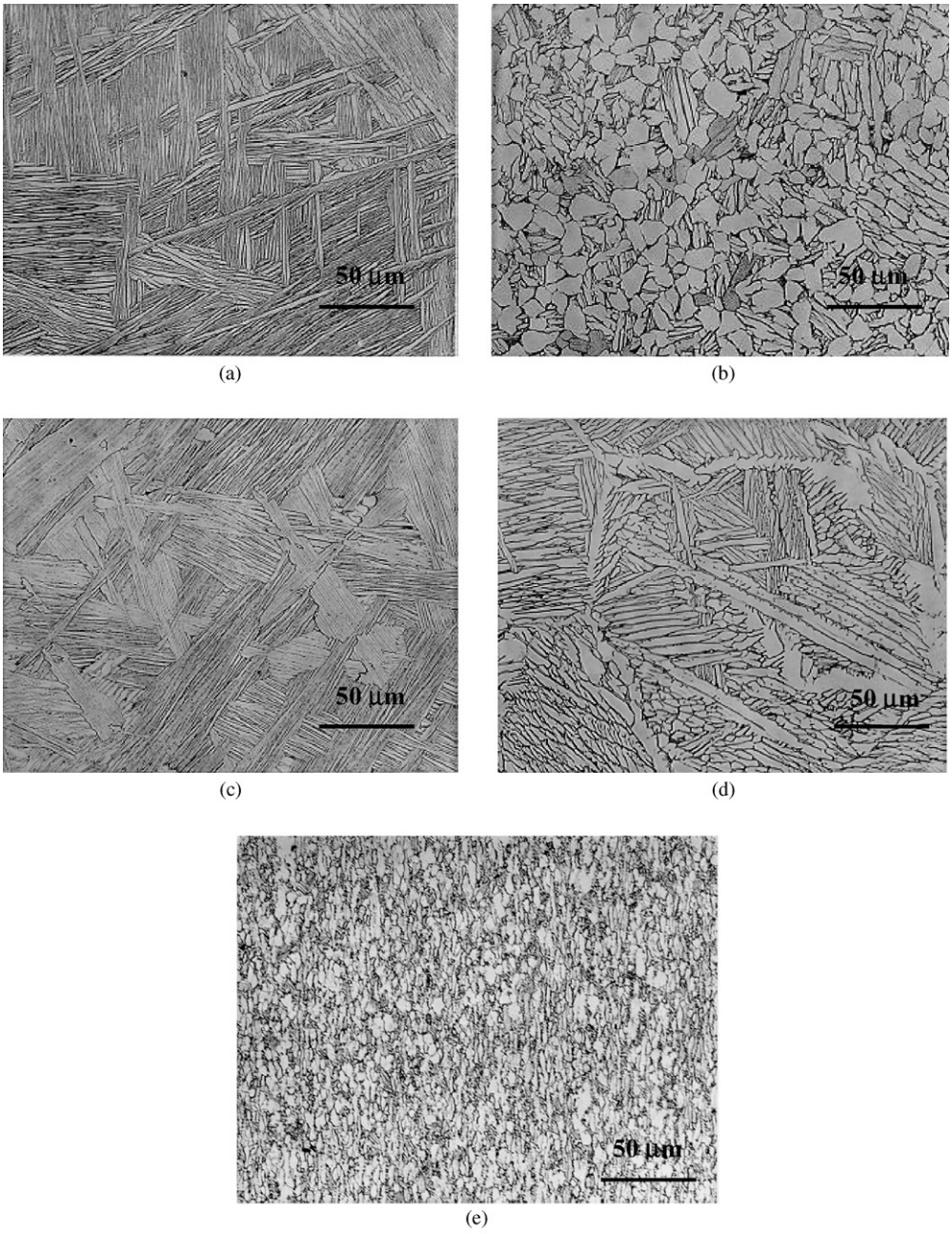

Fig. 2. Microstructure of different targets after hot isostatic pressing and for baseline material: (a) fine lamellar mictrostructure with α (light) and intergranular β (dark) phases corresponding to PREP-nonmilled powder; (b) bimodal (duplex) microstructure consisting of equiaxed grains of "primary" α and transformed β containing platelike α corresponding to PREP-milled powder; (c) fine lamellar microstructure resulting from HIPing of PREP-ELI-nonmilled powder; (d) coarse lamellar mictrostructure corresponding to PREP-ELI-milled powder; (e) microstructure of baseline material in the plane parallel to the axis of bar with elongated α grains in axial direction and intergranular β.

Table 2
Phase content in baseline and HIPed samples

Phases	Baseline (%)	PREP nonmilled (%)	PREP milled (%)	PREP ELI nonmilled (%)	PREP ELI milled (%)
α	66	55	55	62	55
β	34	45	45	38	45

Table 3
Microhardness measurements for different materials

Materials	Baseline	PNM-HIPed	PML-HIPed	ENM-HIPed	EML-HIPed
Microhardness Hv (kg f/mm^2)	348	325	370	329	329

Table 4
Sound speed measurement and calculated results for elastic properties of different materials

Material	No.	V_L (m/s)	V_T (m/s)	Possion's ratio	Young's modulus (GPa)	Shear modulus (GPa)
Baseline (parallel direction)	1-N	6160	3130	0.33	116	44
Baseline (perpendicular direction)	—	6200	3315	0.30	128	49
	2-N	6240	3210	0.32	121	46
	3-N	6190	3080	0.36	113	42
	4-N	6300	3120	0.38	117	44
	W-2	6140	3130	0.33	115	44
PNM	6-N	6140	3190	0.32	115	45
	8-N	6140	3160	0.32	118	45
PML	9-N	6290	3230	0.32	123	47
	10-N	6330	3230	0.32	123	47
ENM	15-N	6210	3190	0.33	117	46
	17-N	6200	3180	0.32	119	45
EML	12-N	6220	3200	0.32	117	46
	13-N	6210	3190	0.32	117	45

V_L is longitudinal and V_T is transverse wave.

being some sort of a "lubricant" during the penetration process, thus reducing the interaction between steel penetrator and titanium target.

A measurement of initial velocity of the projectile was executed by the interruption of two parallel laser beams 152.4 mm apart that were directed onto photodiodes connected to a time interval meter which recorded the transit of the bullet passage (Fig. 5). The terminal velocity of the striker (or plug) was determined from signals generated by the successive closure of two circuits composed of two sets of parallel aluminum foils, each 5 mm apart; the two sets were separated by a distance of 158 mm. This arrangement ensured that the signals were generated by

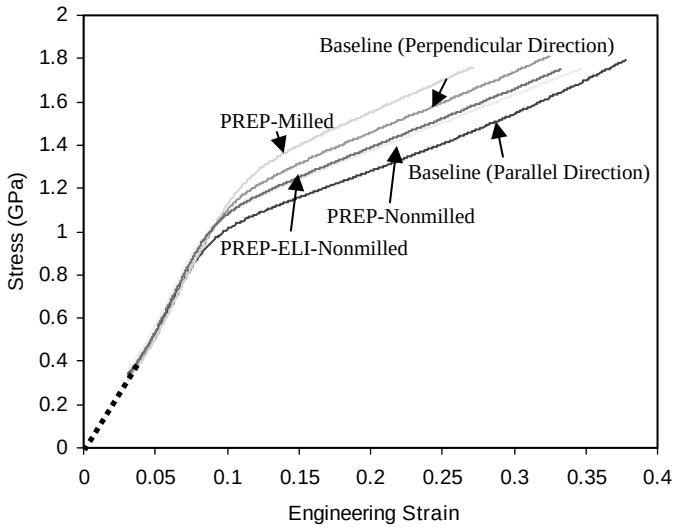

Fig. 3. Stress–strain curves for different target materials in a quasistatic compressive test.

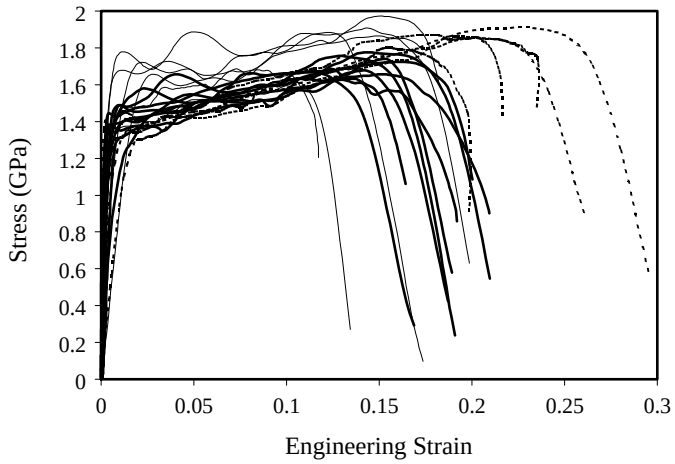

Fig. 4. Stress–strain curves for different target materials from dynamic compression Hopkinson bar tests at a strain rate about 10^3/s; bold solid line corresponds to HIPed PREP-nonmilled powder, fine solid line corresponds to a samples of a baseline material compressed along the direction perpendicular to the axis of the bar; interrupted line corresponds to samples of a baseline material compressed along the direction parallel to the axis of the bar.

the simultaneous contact successively for each set by either the plug of 10 mm length, or by the projectile; no random fragments of sizes smaller than 5 mm could activate this system. Only experiments with holes created by plugs in two aluminum foils aligned with the original line of firing were taken into consideration for calculations of the final velocities of the plugs. The specimens were backed and side-supported by 140 mm diameter 4340 steel rings with central 38 and 40 mm diameter holes, respectively, that prevented motion of the samples relative to the target holder (Fig. 6).

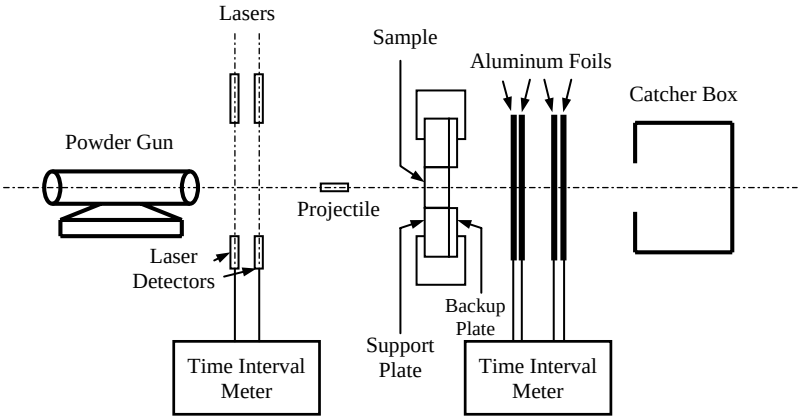

Fig. 5. Experimental set-up for ballistic testing.

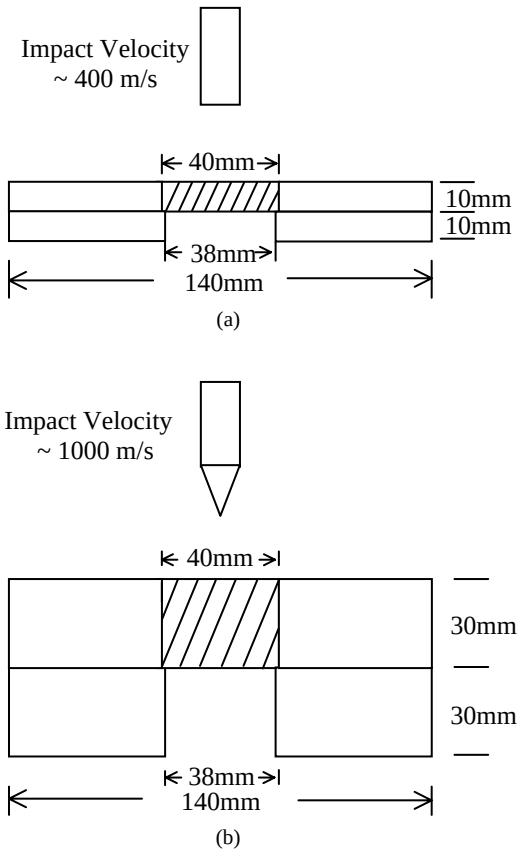

Fig. 6. Geometry for plugging test with (a) blunt projectile and (b) with cylindro-conical projectile.

This entire equipment was mounted on a massive steel table with an approximate mass of 690 kg. A catcher box was located beyond the ballistic facility to capture the projectiles and plugs (Fig. 5). A reliable calibration curve plotting the powder load as a function of initial velocity had been determined from more than 500 shots and was used to establish the initial velocity in a few cases when the measuring equipment failed; the experimental error in this procedure was within $\pm 3\%$.

Impact speeds of the flat-ended striker in the range of about 400 m/s were selected based on two criteria: (1) the test should produce complete perforation of the target and (2) the projectile should remain intact with minimal plastic deformation to ensure that the ballistic performance of the target remains independent of any fracture and/or deformation of the projectile. It was observed that at higher initial velocities, i.e. 500 m/s, the projectile broke for a target thickness of 30 mm without producing perforation. The data from this test are included for comparison. Typically, three or more tests were performed for each kind of material, impact velocity and striker configuration.

The perforated targets had not moved from their original positions in the support plate. Subsequent to the test they were carefully removed for visual and microstructural observations. The targets were cut in the middle along the perforated channel and polished for structural examination under an optical microscope. The plugs were also examined under a scanning electron microscope for fracture patterns developed during shear plugging.

3. Results and discussion

3.1. Experimental results

The perforation process did not completely erode the copper coating on the projectile (as shown in Fig. 7); in fact, a very thin titanium layer was deposited over the copper on the leading edge of the striker. This observation documents that the shear stress due to friction between the target and projectile never exceeds the dynamic shear strength of the deposited copper.

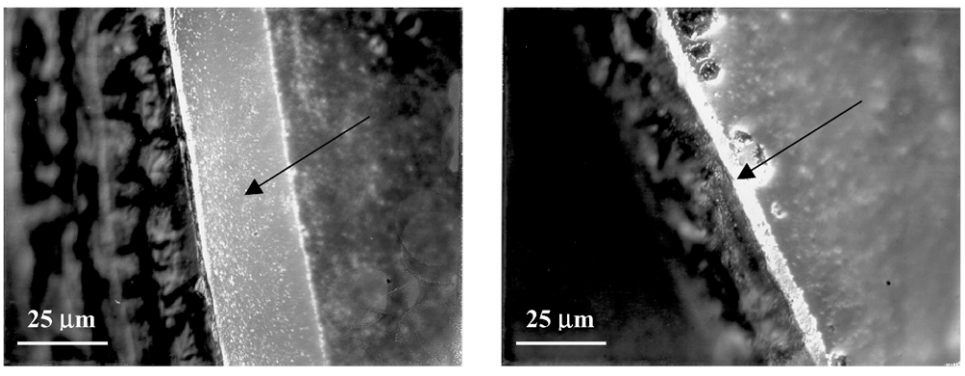

Fig. 7. Copper coating (shown by arrow) on projectile before (a) and after impact (b).

Table 5
Results for ballistic tests with conically-tipped projectiles

No.	Material	Impact velocity (m/s)	Plug velocity (m/s)	Masses (g)		
				Projectile		
				Before tests	After tests	Plug
18-N	Baseline	973	367	30.10	30.95	No plug found
19-N	Baseline	900	290	29.90	30.78	11.25
1-GCN	Baseline	946	—	31.04	31.19	No plug found
2-GCN	Baseline	955	292	31.04	Broken	No plug found
24-N	Baseline	926	284	30.20	30.88	17.442
20-N	PNM-16-02	891	No perforation	30.20	Broken	—
23-N	PNM-15-11	948	259	30.20	30.86	15.494
3-GCN	PNM-05-01	934	257	31.15	Broken	21.1
4-GCN	PNM-05-01	936	104	31.16	Broken	24.791
10-GCN	PML-01-09	917	273	31.15	31.06	No plug found
21-N	ENM-17-02	900*	No perforation	30.90	Broken	–
22-N	ENM-11-11	945	No perforation	31	Broken	–
7-GCN	ENM-13-11	950	387.8	31.17	31.30	Plug is broken
6-GCN	EML-18-11	944	No perforation	31.15	Broken	–

*Initial velocity measurements based on the powder load calibration curve.

Table 6
Results from the ballistic tests with flat projectile including estimated shear strength.

No.	Materials	Impact velocity (m/s)	Crater diameter (mm)	Plug thickness (mm)	Plug mass (g)	Plug velocity (U_f) (m/s)	Averaged shear strength (MPa)
2-N	Baseline	528	13.6	9.6	5.30	487	340
4-N	Baseline	421	12.7	9.3	5.306	276	340
6-N	PNM-15-02	421	12.9	9.9	4.894	177	570
7-N	PNM-15-02	360*	12.8	9.8	4.772	187	570
8-N	PNM-15-02	331	13.1	9.9	5.016	80	570
9-N	PML-19-10	429	13.2	9.9	5.076	83	930
10-N	PML-19-10	430	13.6	10.0	5.944	188	930
11-N	PML-19-10	466	13.1	9.9	5.552	169	930
12-N	EML-05-11	365*	12.9	9.9	5.485	180	400
13-N	EML-05-11	361	13.3	9.9	5.628	219	400
14-N	EML-05-11	375	13.0	9.9	5.341	186	400

*Initial velocity measurements based on the powder load calibration curve.

The results from the tests for the baseline and powder-based materials are compiled in Tables 5 and 6, with an asterisk denoting initial velocity measurements based on the powder load calibration curve. Information contained in these tables includes the initial velocity and mass of the striker, velocity and dimensions of the plug, crater diameter and calculated average shear resistance to penetration based on a simplified model as presented below.

The results for ballistic tests with a conically tipped projectile are presented in Table 5. Usually, more complex fracture mechanisms are involved during the penetration of the conically tipped

projectile [1,28] that may result in different performance of materials in comparison with impact by the flat-ended projectile. With powder-based target materials of 30 mm thickness (Runs 20-N, 21-N, 22-N and 6-GCN), no perforation at all was found upon testing (see for example Fig. 8(c) and (d)). Such behavior was not observed in the baseline material for identical test conditions (Fig. 8 (a) and (b)).

The projectile was broken during the process of target penetration in only one run using the baseline material (Run 2-GCN). In all other cases (18-N, 19-N, 1-GCN, and 24-N), the projectiles did not fracture (Table 5). The opposite tendency is demonstrated in the runs with powder-based materials, where in the majority of runs (3-GCN, 4GCN, 20-N, 21-N, 22-N, and 6-GCN), the projectiles were broken during the process of penetration (Table 5).

In general, four clear differences in the test results between HIPed material and the baseline material need to be mentioned.

First, the plug velocities of HIPed materials are all lower than those of the baseline material except for one case (Run 7-GCN).

Second, the projectiles encounter less resistance in penetrating the baseline material while they have more chances to get broken or trapped inside the crater in HIPed material.

Third, there is no continuos shear localization in HIPed material in the direction of penetration as was a characteristic feature for the baseline material. In the latter, shear localization was

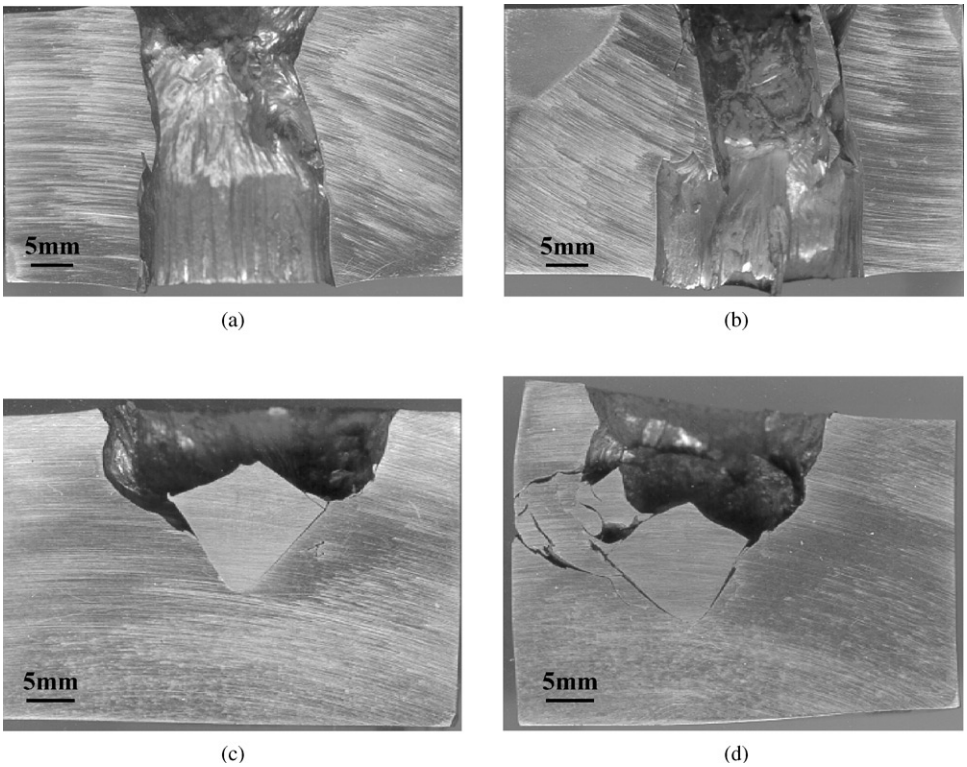

Fig. 8. Perforated targets from baseline material: (a,b) Runs 18N and 19N, respectively; and projectiles trapped inside powder-based targets (c,d) Runs 21N and 22N, respectively.

developed only through about half of the target, being replaced in the distal region by brittle fracture (Fig. 8). It is very interesting that qualitatively similar behavior of powder-based targets in comparison with baseline material (larger diameter of entrance hole and lack of leading shear localization surfaces resulting in smaller penetration depths) was observed during long rod impact [20,21].

Finally, the target fracture is distributed over a greater volume in the beginning of the penetration process causing the diameter of the entrance holes in the powder-based materials (Fig. 8(c) and (d)) to be larger than the corresponding diameter in the baseline material (Fig. 8(a) and (b)). These four points indicate that HIPed material have a better ballistic performance in conically-tipped projectile tests.

The plug geometry from powder-based material for flat-ended impact is depicted in Fig. 9 (Runs 7-N, 8-N, 9-N, 10-N, 14-N, 15-N, 16-N, 17-N)) for a range of projectile velocities from 360 to 465 m/s (see Table 6). In addition, this figure shows the corresponding plugs obtained from the baseline material (Runs 2-N and 4-N). The latter are nearly cylindrical in contrast to the powder-based plugs which are irregular with sharply defined regions of slanted material produced by additional fragmentation when the compressive stresses induced by the impact in the plug are relieved by ejection. The incipient stage of this phenomenon is demonstrated in Fig. 10(a) where the edge of the crater was separated but still attached at one point (Run 15-N). The difference in shape for the corresponding baseline material (Run 4-N) is indicated in Fig. 10(b) where some smaller separated crater fragments attached at the base to the target were found. In other samples from the baseline material, no such fragments were observed. This qualitative difference in behavior demonstrates that shear localization in the baseline material dominates the entire process of plug formation. On the other hand, in the powder-based material, fracture also plays a significant role in the perforation process. A reduction in the thickness of the plug relative to the target of 2–3% for the powder-based material was noted; this is attributed to the initial compressive phase of the impact process before shearing ensues. In general, materials produced from ELI powder did not exhibit different behavior in comparison with PREP powders under shear-induced plugging.

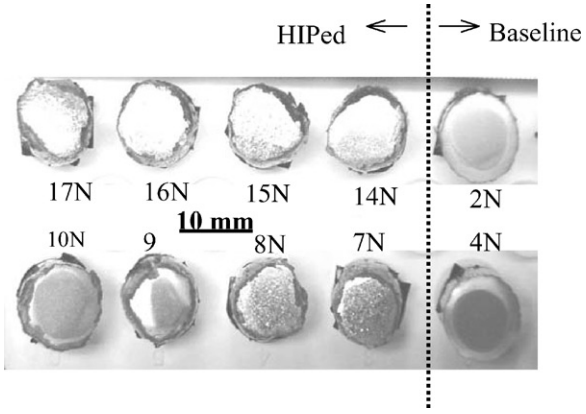

Fig. 9. Shear plugs after ballistic testing of 10-mm thick targets with flat projectile. Notice the cylindrical cross section of MIL-T-9047G samples (far right) and the uneven cross section of plugs from HIPed samples. The plugs are viewed from the free surface of the sample.

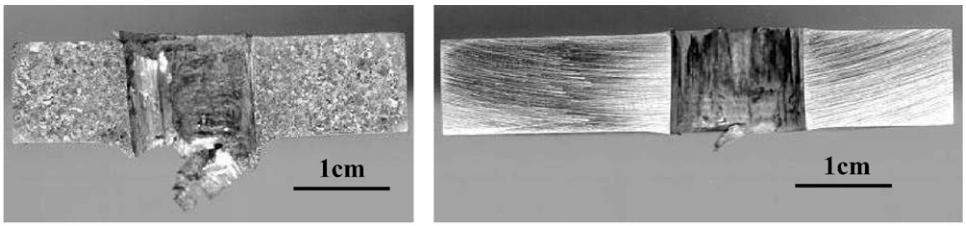

Fig. 10. The crater wall and separated crater fragments connected at the base in (a) powder based (Run 15-N) and (b) baseline (Run 4-N) materials. Notice the difference between fracture on the edges of the walls in the different targets.

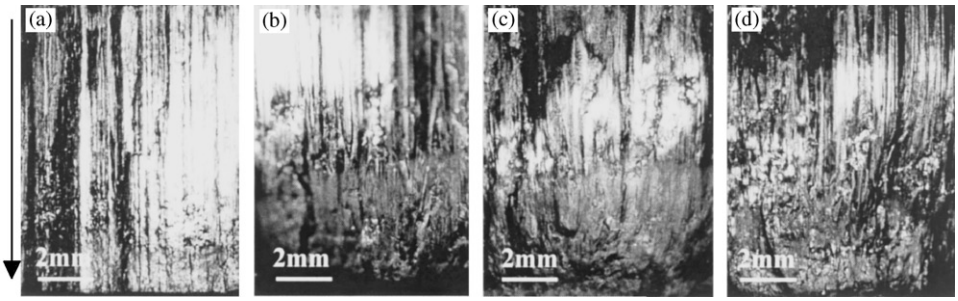

Fig. 11. Striations on plugs from (a) baseline and HIPed materials (b) PNM, (c) PML and (d) ENM targets. Direction of the impact is shown by arrow.

In the baseline material, the lateral surface of the plugs was characterized by clearly identifiable parallel striations with an amplitude up to 200–300 μm (Fig. 11a) represented by two superposed quasi-harmonic structures with a higher frequency corresponding to a smaller amplitude (wavelengths ranging from 2 to 50 μm). In contrast, the striations in the powder-based material extend only a few millimeters into the plug; beyond this position, they are replaced by the fracture pattern as shown in Fig. 11(b)–(d). This replacement of a thin shear localization layer in the direction of penetration by more volume-distributed fracture results in the deviations from cylindrical geometry of the shape of the exit hole and plugs from powder-based targets (Fig. 9).

In general, the plug velocity of the powder-based material was substantially smaller than that of the baseline sample (Table 6). A single exception was found in one test of a series of three identical shots where the plug velocity was substantially greater. No explanation for this anomaly can be suggested.

3.2. Penetration and plug formation with conically tipped projectiles

In the case of conically tipped projectiles striking 30-mm thickness powder-based targets, usually no plugs in the conventional sense were produced (Fig. 8(c) and (d)); only fractured pieces from the region of the crater were recovered. In half of the tests, no perforation of the 30-mm thick target could be achieved in spite of an initial velocity more than twice as great as that used in the plane-ended impacts with 10 mm targets. The crater diameters at the impact side were

invariably substantially larger than the diameter of the projectile, and in a number of instances, this also occurred on the distal surface. In some tests, an incipient plug could be discerned, located in the central region of the target that exhibited the imprimature of the conical projectile geometry. In one instance, where perforation nearly eventuated, the material removed from the target split into two parts. Fractures were evident both in the target and in the recovered ejecta.

The penetration process is clearly totally different from that observed after the impact of similar cylindro-conical strikers on thin, ductile aluminum plates [28,29]. It is also not depicted by the analytical representation of the perforation of such plates by this type of striker, analyzed by Landkof and Goldsmith [30] for thin plates where the evolution of fractures resulted in the formation of petals, permitting the passage of this projectile. The random nature of the crater geometry and ejecta formation in the present tests would seem to indicate the existence of a much more complex phenomenon for this type of collision in targets of medium thickness than in case of flat-ended impact. This includes the distinct possibility that significant changes in behavior could result from slight deviations in the obliquity of the collision.

Results from the tests with conical projectiles are presented in Table 5. In several experiments with HIPed material, the projectiles could not be recovered intact. Often, the projectile had broken into several pieces. In a few instances with powder-based targets, the projectile was trapped inside the target without perforation or plugging (Fig. 8(c) and (d)). This behavior was typical only for HIPed targets and was not observed in the baseline material.

The velocity of the plugs for the baseline MIL-T-9047G target is ~ 290 m/s for two samples and 367 m/s in the third. It is assumed that interfaces in the targets (see Fig. 6) do not influence the results on the exit plug velocities and that the present results are also valid for large scale targets prepared from powders (the HIPing process ensures this scaling). It is based on the experimental fact that no relative movement of the sample and support rings was noticed in the cases of penetration where the velocity of the plug was measured with central impact for cases presented in the tables. An additional test to assess the effectiveness of the press-fitting was performed. A plug-fitting velocity of 284 m/s was also observed for a 140-mm diameter uniform target of the baseline material which is practically the same as for the sample with diameter 40 mm supported by a ring. This also supports the hypothesis that the mechanical fixing of the targets did not influence the present results.

The observed plug velocities of HIPed nonmilled PREP (PNM) samples of ~ 257 m/s are lower than those observed for any of the baseline samples. The smaller plug velocity of 104 m/s observed for one of the PNM samples also coincided with a heavy deformation of the backup plate. It is likely that the deformation of the support plate in this case may have contributed to the loss of energy of the plug.

The plug velocities in targets HIPed from nonmilled ELI (ENM) powder exhibited unusual behavior (see Table 5). In one experiment (ENM-13–11) the velocity value was relatively high and in others, perforation was not observed (experiments ENM-17–02 and ENM-11–11).

3.3. Penetration and plug formation caused by shear localization with flat-ended projectiles

In the case of flat-ended projectile impact on targets from baseline material with 10-mm thickness, the interior of the target craters was visually smooth. The entrance and exit holes were circular and concentric, with the distal side exhibiting a slightly larger diameter and some small,

random irregularities on their peripheries. The plugs generated for the baseline material were of nearly cylindrical shape, while those of the HIP samples exhibited a more irregular contour (Fig. 9). All displayed a slight, uniform enlargement of the diameter towards the distal side so as to form a frustum of a cone. No additional deformation was produced in the plugs during the process of recovery.

A noncylindrical shape of the exit hole was a typical feature for tests with powder-based materials. A similar geometry of the exit hole produced by the perforation of a blunt hard-steel striker is due to the formation of cracks in the target, which consisted of medium carbon steel (Fig. 13 in paper by Goldsmith and Finnegan [27]). The cause of this phenomenon is the brittle nature of the target, which dominates the failure process and overshadows the shearing action. The difference between the steel and Ti–6Al–4V is the extension of radial cracks in the steel beyond the region of fragment detachment, whereas the Ti–6Al–4V target did not exhibit this feature.

Based on the initial (10 mm) and final thickness of the plugs (Table 6) a smaller compression of (1–2% strain) is generated for powder-based materials in comparison with that of 4–7% in the baseline material.

The lateral surface of all these plugs exhibited linear and parallel striations around the entire periphery in the direction of motion (Fig. 11). Such patterns have not been noted in any of the hundreds of plugs generated by impact of blunt strikers on a variety of aluminum alloy or steel targets. A possible cause for the formation of this striated pattern is the presence of the terminal crater surface irregularities with relatively high strength which could generate these hills and valleys in the plug surface liquified by the temperature increase induced by the shear localization process. However, this hypothesis is tenuous in view of the irregular distribution of the target protrusions and the extremely uniform appearance of the striations. No other obvious explanation for this observation is available; perhaps geometrical instability of the cylindrical shear localization surface coupled with the extreme temperature/pressure condition and possibly variations induced by wave propagation could play a role in inducing the periodic pattern of this phenomenon. This feature requires further investigation.

The impact surfaces of the baseline material plugs are smooth, virtually polished, while those of the compacted powder samples are noticeably more irregular. Some mushrooming combined with a slight turning of the material backwards is evident on the distal end and, in some cases, but far less prominently so on the impact side.

After impact by the flat-ended projectile, the targets were cut into two pieces along the penetration channel and polished for microstructural examination. The orientation of the grains in the targets from baseline materials along the bar axis is due to a forging process and is aligned in the direction of the bullet trajectory. The dynamic properties of the textured baseline material in the direction perpendicular and parallel to the forging direction are different [24]. Typical areas close to the channel wall created by the main shear band propagating in the impact direction for the two types of materials are shown in Figs.12 and 13. It is evident that in both cases the area corresponding to the main shear band is not uniform and contains the pattern of locally developing secondary shear bands. This periodic pattern of secondary shear bands with a thickness of 2 μm and spacing of about 10–15 μm could be noticed in the baseline material (Fig. 12). Shear bands in HIPed targets have a larger thickness (Fig. 13). The shear bands in powder-based material propagate 450 μm into the matrix.

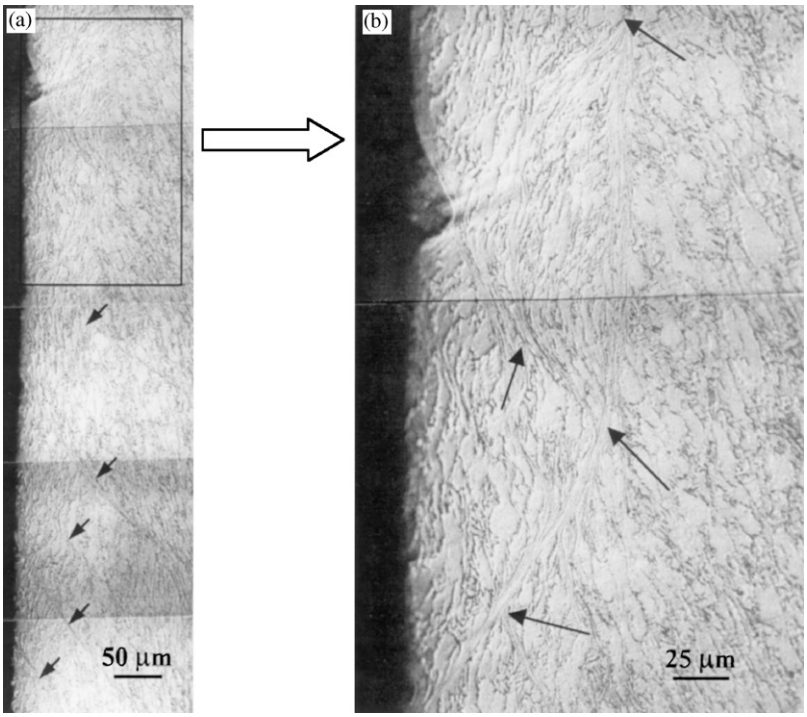

Fig. 12. (a) Periodic pattern of secondary shear bands (shown by arrows) in baseline MIL-T-9047G sample after ballistic testing (Run W-2, velocity of projectile 360 m/s) with flat projectile; and (b) bifurcation of shear bands at the top part of the same sample.

The branching and bifurcation of shear bands and interaction with one another are a distinct and a common feature of the HIPed targets (Fig. 13) relative to the baseline material (Fig. 12). The example of the shear bands interacting with each other in a powder-based material is shown in Fig. 13(b). We consider this feature being mainly responsible for the enhanced ballistic performance of HIPed materials.

The dimple structures characteristic for ductile fracture in the baseline material and in the HIPed samples are shown in Fig. 14. Both samples have almost the same dimple size, distribution and shape, similar to those observed by Grebe et al. [31]. The baseline material has dimples mostly aligned in the same direction, while in the HIPed samples they appear to be in the form of small clusters. This shows that these materials exhibit similar ductile fracture. At the same time, twins are regularly found in HIPed samples and never found in baseline samples.

The experiments with a target thickness of 30 mm from the baseline material did not result in plugging under flat-ended projectile impact at a velocity of 541 m/s (Fig. 15). Instead, a shear band with cylindrical geometry (with cracks close to the impact point) was found to propagate up to a depth of 10 mm into the body, starting from the edge of the crater of 2 mm depth on the impacted side of the target. The thickness of the circular shear band area decreases with the depth, starting with 23 μm. At a depth of 10 mm, the thickness of the shear band was 5 μm and its dependence on depth can be approximated as a linear function. This experiment represents the

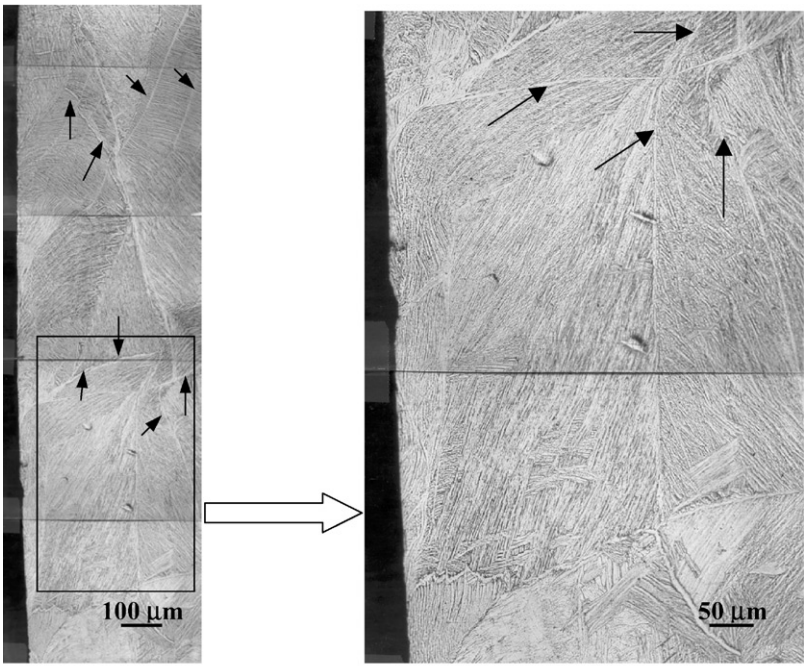

Fig. 13. (a) Pattern of secondary shear bands (shown by arrows) in HIPed material (PREP-nonmilled (PNM), Run 8N); and (b) bifurcation of shear bands at the bottom part of the same sample after ballistic testing with a flat projectile.

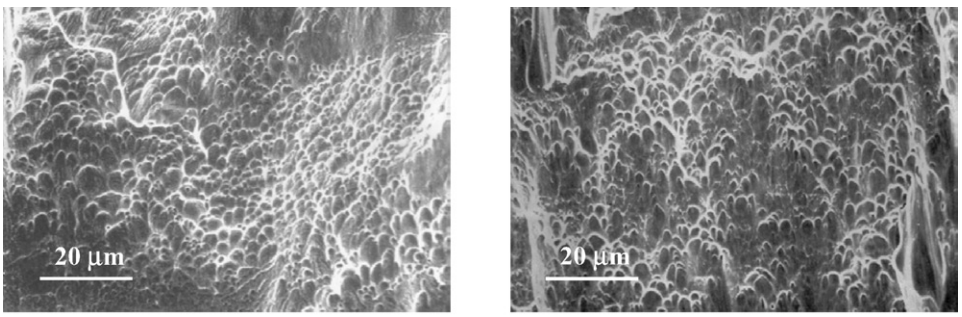

Fig. 14. Characteristic dimples in: (a) PNM (nonmilled, HIPed powder-based material, Run 15N); and in (b) baseline sample (Run W2, velocity of flat ended projectile 360 m/s).

intermediate stage of plug formation for flat projectile impact and can be used for numerical modeling of nucleation of shear localization and subsequent perforation in Ti–6Al–4V.

3.4. Evaluation of nominal shear resistance to penetration

Three separate stages of the plugging phenomenon have been described by Goldsmith and Finnegan [4] that consist of initial compression, subsequent motion of the plug up to ejection, and

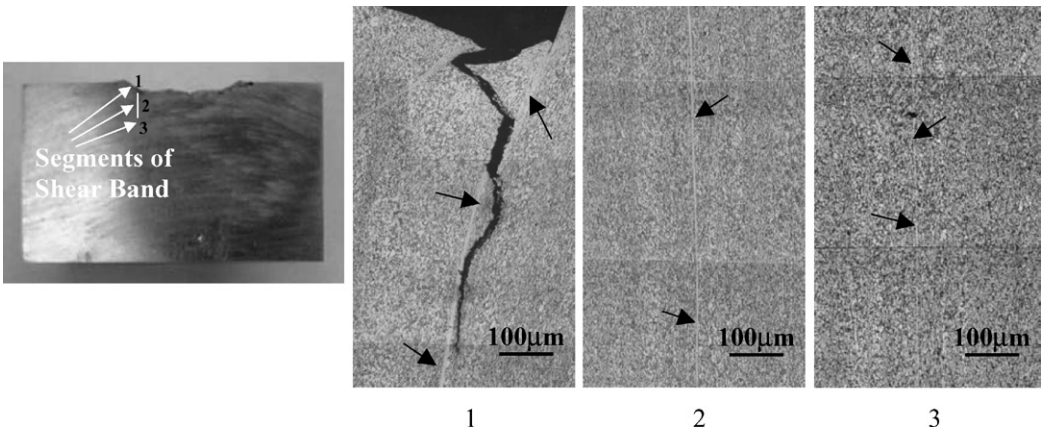

Fig. 15. Segments of shear band (1, 2 and 3) propagating into the target 5–6 mm along the impact direction from the surface of the target in the baseline material MIL-T-9047G; sample with thickness 30 mm after impact with flat projectile, velocity 528 m/s.

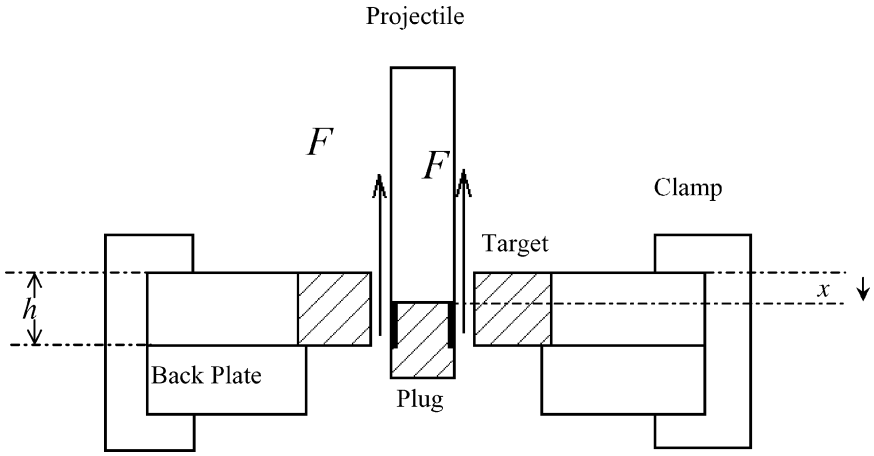

Fig. 16. The definition of the parameters used to estimate the shear strength of Ti–6Al–4 V samples.

traverse of the target by the projectile. Here, the determination of the average shear resistance to penetration is based on the model shown in Fig. 16, which encompasses the second and third stages of this representation. It combines the forces acting on the projectile and plug and assumes the same initial and terminal velocity for these components, i.e. it ignores the plug compression during which the plug acquired the velocity of the striker after initial impact. The analysis is similar to that presented by Holt et al. [17]. The major problem with this model of plugging is that it does not account for a bulk distributed fracture of the target, which cannot be described by shear stresses. Nevertheless the results of calculations based on this simplified model can produce additional insight into comparative behavior of the investigated materials.

This assumption is made only for the stage of penetration when the projectile forcefully drives a plug, until the latter is separated from the target. It was not assumed that projectile and plug have

the same final exit velocities. After plug separation, the projectile continues to interact with the target, and that is why its exit velocity may be quite different than the exit velocity of the plug. But this stage of perforation is not considered.

The relevant equation for force F caused by shear resistance of the target to plug motion and friction on the projectile target interface is given by

$$F(x) = -\pi D(h-x)\tau - \pi D x \tau_c, \tag{1}$$

where D is the diameter of the plug, h is the thickness of the target, x is displacement of the plug, τ and τ_c are shear resistance of the target and friction between projectile and target, respectively (positive numbers). The shear strength of copper can be used to approximate the maximal possible friction force between the projectile and the copper-coated target. This is based on the experimental fact that the copper coating was not totally removed (Fig. 7), and, furthermore, a very thin titanium layer was deposited on the surface of the remaining copper coating. The remnants of copper were found on the wall of the craters.

The equation of motion for the projectile-plug system follows from Eq. (1)

$$m\frac{\mathrm{d}\upsilon}{\mathrm{d}t} = F(x) = -\pi D(h-x)\tau - \pi D x \tau_c, \tag{2}$$

where m and υ are the combined mass of projectile and plug and their velocity, respectively. Eq. (2) can be integrated using the equation $\mathrm{d}x = \upsilon\,\mathrm{d}t$

$$m\int_{U_0'}^{U_f} \upsilon\,\mathrm{d}\upsilon = -\int_0^h [\pi D(h-x)\tau + \pi D x \tau_c]\,\mathrm{d}x. \tag{3}$$

Here the initial velocity υ_0 of the projectile-plug system is designated as U_0' and is equal to

$$U_0' = \frac{M_0}{M_0 + M_p} U_0, \tag{4}$$

where U_0 is the final velocity of the projectile-plug system, and U_f will be designated as the final velocity, while M_0, M_p are masses of the projectile and the plug, respectively.

Based on the measured initial velocity of the projectile (U_0) and final velocity of the plug (U_f), the averaged shear resistance τ to plugging can then be expressed as

$$\tau = \frac{1}{\pi D h^2}\left(\frac{M_0^2}{M_0 + M_p}U_0^2 - (M_0 + M_p)U_f^2\right) - \tau_c. \tag{5}$$

The copper in the coating undergoes high strain and high strain rate flow during the penetration process. The flow stress of copper (the yield strength for normal conditions is about 120 MPa) is highly strain- and strain-rate dependent [32]. For example, at a plastic strain of 0.15, it increases from 200 MPa at strain rate of 10^{-5}/s to about 360 MPa at a strain rate of 10^4/s [32,33]. Since in the present experiments the copper layer is deformed mostly under high strain conditions, the upper value of shear strength of copper in Eq. (5) is assumed to be one-half of the average of the last two values, $\tau_c = 140$ MPa. The initial thickness of the target ($h = 10$ mm) and the projectile diameter ($D = 12.73$ mm) were used in calculations despite the fact that the plug thickness was slightly smaller than h and different crater diameters were observed in the experiments (see Table 6). The calculated (average for each group of experiments) shear resistance values based on Eq. (5) are shown in the Table 6.

The evaluated average shear resistance of the baseline material (340 MPa) in the present experiments is comparable to the value of 335 MPa obtained in the reverse-ballistic impact configuration by Holt et al. [17] for commercial Ti–6Al–4V alloy.

The average shear resistance (570 MPa) of the powder-based material (PREP powder) is higher than in the baseline material but it is below one-half of the flow stress in Hopkinson bar experiments [23,24]. For example, at a strain rate of 6.7×10^3/s, the flow stress for material processed from nonmilled powder is about 1300 MPa. This means that the calculated shear resistance in penetration experiments can be interpreted mainly as a result of localized shear flow on the periphery of the plug.

The calculated resistance to penetration of targets prepared from milled PREP powder (930 MPa) was larger than one-half of the flow stress for dynamic compression in a Hopkinson bar test (1700 MPa at a strain rate of 5.1×10^3/s [23]). Shear localization in ballistic tests results in a high temperature inside the shear zone that will only decrease average material shear strength in comparison with the expected value based on Hopkinson bar tests. This high value of the calculated shear strength obtained based on the simple model presented indicates that, despite the apparent classical geometry of plugging, other mechanisms of energy dissipation additional to shear localization are effective during the penetration process in the targets prepared from milled PREP powder. The shear resistance obtained based on the simple model (Eq. (5)) represent the overall behavior of a target averaged over very different states of the material (from solid to possible melting state) during different stages of the penetration process. It effectively includes all processes of energy dissipation due to plastic deformation and fracture in addition to shear localization.

Targets prepared from ELI milled powders had an average shear strength (400 MPa) comparable to the strength of the baseline material in the present experiments and in experiments by Holt et al. [17]. The results for runs with targets processed from nonmilled ELI powders are not included in Table 6 because there is not sufficient experimental data to arrive at reasonable conclusions.

The plug velocity for the baseline material in Run 2-N with a projectile velocity 528 m/s was very high, resulting in a negative shear strength that demonstrates the restrictions of the present model in cases where the exit velocity of the plug is too close to the velocity of the projectile. In the majority of the present experiments, the plug velocity was substantially lower than the initial velocity of the projectile.

The computed shear resistance using the present simple model can be used only for comparison of the behavior of different materials under similar conditions of impact. More sophisticated considerations for plugging based on a thermo-viscoplastic model of the material and using a Lagrangian finite element code can be found in [34].

4. Conclusions

The impact of cylindro-conical and flat-ended strikers of 31 g mass at velocities ranging from 360–430 m/s (plane) and 890–950 m/s (conical) on hot isostatically compacted texture-free targets from powders of titanium alloy (Ti–6Al–4V) were compared with similar tests on baseline material of the same alloy (MIL-T-9047G, bar, forged, annealed).

In half of the experiments with 30-mm thick targets from powder-based materials and cylindro-conical projectiles, no perforation was achieved and the projectile invariably fractured into many pieces with only a few components recovered. In contrast, the baseline material targets of the same thickness were perforated in all tests with only a slightly deformed striker in the majority of cases. In the tests where powder-based material was perforated, the plug velocities as a rule were lower than plug velocities in the baseline material. This difference in the behavior is explained by greater volume distributed fractures in the initial stages of penetration and larger resistance to shear localization in powder-based material. Microstructural differences (like higher content of β phase and remnants of particles boundaries) result in higher strength, lower ductility and complex pattern of shear bands. This is consistent with material behavior during ballistic tests with long rod projectiles [24].

At the same time it should be emphasized that a relation between microstructural features and ballistic performance is not clarified even for traditionally processed Ti–6Al–4V alloy and certainly more research is needed with material prepared from powder to establish such a correspondence.

The impact of a flat-ended striker on the 10 mm thick target results in shearing of a plug along a cylindrical surface approximating the striker periphery, but slightly larger, and always terminating in plug ejection with concomitant perforation of the striker. The velocity of plugs from powder-based materials were as a rule smaller than the velocities corresponding to the baseline material. Powder-based materials demonstrated fractures distributed over a larger volume near the end of plugging and exhibited a qualitatively different behavior with respect to shear localization (multiple shear banding, branching, larger thickness of shear band). No noticeable improvement of ballistic performance was observed for materials from ELI grade powder in comparison with PREP powders. Targets hot isostatically pressed (HIPed) from ball milled powder had a larger shear resistance than material processed from nonmilled powder. This is consistent with higher flow stress observed in the Hopkinson bar test for material prepared from milled powder [23]. The averaged shear resistance to the plug formation of the powder-based materials (nonmilled PREP and milled ELI powders) was less than one-half of the dynamic compressive strength of the same material and was larger than for baseline sample of MIL-T-9047G. The materials prepared from milled PREP powders exhibited the largest shear strength, which is consistent with their behavior in Hopkinson bar experiments. In the latter case, the shear strength was larger than one-half of the dynamic compressive strength of the same material indicating the presence of other mechanism(s) of dissipation in addition to the one-dimensional shear localization in the striking direction.

Finally, HIPed targets from Ti–6Al–4V powders exhibit a good ballistic performance against perforation and plugging in comparison with the baseline material (MIL-T-9047G). This allows the development of composite armor materials based on powder technology, which can produce products with complex shape suitable for the incorporation of different devices inside armor for multifunctional purposes.

It is reasonable to expect that the HIPed material will be useful against jacketed small arms projectiles, AP and/or Ball because it demonstrated better performance for very different geometries of impact—blunt projectiles, conically tipped projectiles and long-rod projectile [20,21].

Acknowledgements

The support provided by the Army Research Office under MURI program DAAH004-96-10376 (Program Manager Dr. David Stepp) is highly appreciated. We also acknowledge Mr. Benjamin Bourne and Mr. Jerald Jung of UC Berkeley for their help during ballistic testing and reviewers for very helpful suggestions.

References

[1] Goldsmith W. Impact: the theory and physical behaviour of colliding solids. London: E Arnold, 1960.
[2] Goldsmith W. Bouncing from one collision to the next. Appl Mech Rev 1999;52:R27.
[3] Backman ME, Goldsmith W. The mechanics of penetration of projectiles into targets. Int J Eng Sci 1978;16:1.
[4] Goldsmith W, Finnegan SA. Penetration and perforation processes in metal targets at and above ballistic velocities. Int J Mech Sci 1971;13:843.
[5] Johnson W. Impact strength of materials. London: E Arnold, 1972.
[6] E. Martel, S.A. 1897; 2.
[7] Alekseevski VP. Penetration of a rod into a target at high velocity. Combust Explos Shock Waves 1966;2:63.
[8] Me-Bar Y, Rosenberg Z. On the correlation between the ballistic behavior and dynamic properties of titanium-alloy plates. Int J Impact Eng 1997;19:311.
[9] Montgomery JS, Wells MGH, Roopchand B, Ogilvy JW. Low-cost titanium armors for combat vehicles. JOM 1997;45.
[10] Burkins M, Love W. Effect of annealing temperature on the ballistic limit velocity of Ti–6Al–4V ELI. In: Proceedings of 16th International Symposium on Ballistics, San Fransisco, CA, 23–27 September, 1996.
[11] Gooch WA, Burkins MS, Frank K. Ballistic performance of titanium against laboratory penetrators. In: Proceedings of First Australian Congress on Applied Mechanics, Melbourne, Australia, 21–23 February, 1996.
[12] Rupert NL, Grace FI. Impact studies of rod projectiles against titanium and steel targets. In: Murr LE, Staudhammer KP, Meyers MA, editors. Metallurgical and materials applications of shock-wave and high-strain-rate phenomena. Amsterdam: Elsevier Science, 1995. p. 257.
[13] Huang W, Murr LE, Niou C-S, Rupert NL, Grace FI. Metallurgical studies of deformation and failure patterns from targets impacted by log-rod penetrators. In: Murr LE, Staudhammer KP, Meyers MA, editors. Metallurgical and materials applications of shock-wave and high-strain-rate phenomena. Amsterdam: Elsevier, 1995. p. 265.
[14] Bless SJ, Gooch WA, Satapathy S, Lee M. Penetration resistance of titanium and ultra-hard steel at elevated velocities. Int J Impact Eng 1997;20:121.
[15] Meyer LW, Krueger L, Gooch W, Burkins M. Analysis of shear band effects in titanium relative to high strain-rate laboratory/ballistic impact tests. J Phys IV France 1997;7:C3–415.
[16] Weerasooriya T, Magness L, Burkins M. High strain-rate behavior of two Ti–6Al–4V alloys with different microstructures. In: Murr LE, Staudhammer KP, Meyers MA, editors. Fundamental issues and applications of shock-wave and high-strain-rate phenomena. Amsterdam: Elsevier, 2001. p. 33.
[17] Holt WH, Mock Jr. W, Soper WG, Coffey CS, Ramachandran V, Armstrong RW. Reverse-ballistic impact study of shear plug formation and displacement in Ti–6Al–4V alloy. J Appl Phys 1993;73:3753.
[18] Me-Bar Y, Shechtman D. On the adiabatic shear of Ti–6Al–4V ballistic targets. Mater Sci Eng 1983;58:181.
[19] Mazeau C, Beylat L, Longere P, Louvigne PF. On the quantitative evaluation of adiabatic shear banding sensitivity of various titanium alloys. J Phys IV France 1997;7:C3–429.
[20] Nesterenko VF, Indrakanti SS, Brar S, Gu Y. Long rod penetration test of hot isostatically pressed Ti-based targets. In: Furnish MD, Chhabildas LC, Hixson RS, editors. Shock compression of condensed matter. Melville, NY: AIP, 1999. p. 419.
[21] Nesterenko VF, Indrakanti SS, Brar S, Gu Y. Ballistic performance of hot isostatically pressed (HIPed) Ti-based targets. Key Eng Mater 2000;177–180:243–8.

[22] Nesterenko VF, Indrakanti SS, Goldsmith W, Gu Y. Plug formation and fracture of hot isostatically pressed (HIPed) Ti–6Al–4V targets. In: Staudhammer KP, Murr LE, Meyers MA, editors. Fundamental issues and applications of shock-wave and high-strain-rate phenomena. Amsterdam: Elsevier, 2001. p. 593.
[23] Nemat-Nasser S, Guo W, Nesterenko VF, Indrakanti SS, Gu Y. Dynamic response of conventional and hot isostatically pressed Ti–6Al–4V alloys: experiments and modeling. Mech Mater 2001;35:425.
[24] Gu Y, Nesterenko VF, Indrakanti SS. Ballistic testing and high-strain-rate properties of hot isostatically pressed Ti–6Al–4V. In: Furnish MD, Thadhani NN, Horie Y, editors. Shock compression of condensed matter. Melville, NY: AIP, 2002. p. 1294.
[25] Lutjering G, Williams JC, Gysler A. Microstructure and mechanical properties of titanium alloys. In: Li JCM, editor. Microstructure and properties of materials. Singapore: World Scientific, 2000. p. 1.
[26] Nesterenko VF, Indrakanti SS. Tailoring of microstructure of Ti–6Al–4V alloy by combined cold plastic deformation and hot isostatic pressing. In: Khan AS, editor. Constitutive and damage modeling of inelastic deformation and phase transformation, Proceedings of the Plasticity'99. Fulton Maryland: Neat Press, 1999. p. 251.
[27] Yong L, Nesterenko VF, Indrakanti SS. Modified Arzt–Ashby–Easterling model for powder consolidation. Met Mater 1998;4:336.
[28] Goldsmith W, Finnegan SA. Normal and oblique impact of cylindro-conical and cylindrical projectiles on metallic plates. Int J Impact Eng 1986;4:83.
[29] Goldsmith W. Initiation of perforation in thin plates by projectiles. In: Reid SR, editor. Metal forming and impact mechanics W. Johnson commemorative volume. Oxford: Pergamon Press, 1985. p. 271.
[30] Landkof B, Goldsmith W. Petalling of thin metallic plates during penetration by cylindro-conical projectile. Int J Solids Struct 1985;21:245.
[31] Grebe HA, Pak HR, Meyers MA. Adiabatic shear localization in titanium and Ti–6Al–4V alloy. Metall Trans A 1985;16A:761.
[32] Meyers MA. Dynamic behavior of materials. New York: Wiley, 1994.
[33] Follansbee PS, Kocks UF. A constitutive description of the deformation of copper based on the use of the mechanical threshold stress as an internal state variable. Acta Metall 1988;36:81.
[34] Chen L, Li Y-C, Wang LL. A computational investigation of adiabatic shear plugging based on thermal-viscoplastic instability. Acta Mech 1997;126:127.